Dynamics of cryogen deposition relative to heat extraction rate during cryogen spray cooling.

Wim Verkruysse*[a], Boris Majaron[a,b], Guillermo Aguilar[a,c], Lars O Svaasand[d] and J. Stuart Nelson[a],

[a] Beckman Laser Institute and Medical Clinic, Univ. of California, Irvine, CA 92162

[b] Jozef Stefan Institute, Jamova 39, SI-1000 Ljubljana, Slovenia

[c] Chemical and Biochemical Engineering and Materials Science, Univ. of California, Irvine, CA 92162

[d] University of Trondheim, N-704 Trondheim Norway

ABSTRACT

Goal is to investigate how delivery nozzle design influences the cooling rate of cryogen spray as used in skin laser treatments. Cryogen was sprayed through nozzles that consist of metal tubes with either a narrow or wide diameter and two different lengths. Fast-flashlamp photography showed that the wide nozzles, in particular the long wide one, produced a cryogen jet (very small spray cone angle) rather than a spray (cone angles of about 15° or higher) and appeared to atomize the cryogen less finely than the narrow nozzles. We measured the cooling rate by spraying some cryogen on an epoxy-block with thermocouples embedded. The heat extraction rate of the wide nozzles was higher than that of the narrow nozzles. The results suggest that finely atomized droplets produced by the narrow nozzles do not have enough kinetic energy to break through a layer of liquid cryogen accumulated on the object, which may act as a thermal barrier and, thus, slow down heat extraction. Presumably, larger droplets or non-broken jets ensure a more violent impact on this layer and therefore ensure an enhanced thermal contact. The margin of error for the heat extraction estimate is analyzed when using the epoxy-block. We introduce a complementary method for estimating heat extraction rate of cryogen sprays.

Keywords: cooling selectivity, spurt, heat transfer, port wine stain, cryogen

1. Introduction

In laser treatment of skin lesions, such as port wine stain (PWS), two competing absorbers of light can be identified: melanin (in the epidermis) and oxy-hemoglobin (in the blood vessels which are the targets). Because high temperatures in the basal layer of the epidermis are associated with a risk on scarring, blistering or dys-pigmentation. This risk poses an upper limit to the laser radiant exposure. Cryogenic spray cooling (CSC) reduces the temperature of the epidermis, thus allowing for a laser pulse with higher energy [1,2]. As deeper structures (target blood vessels) are cooled less than the epidermis, the high energy laser pulse causes more damage to the targets while maintaining the same degree of safety in terms of risk of scarring.

Since the first commercial implementation of CSC several years ago (DCD, Candela, Wayland MA) this cooling method has been increasingly used. Clinical results of PWS laser treatment for example, have improved in terms of better blanching [2,3] as well as reduced pain [4]. Also, treatment of hemangiomas [5] and rhytides [6] has benefited from using CSC. Despite its wide use, the exact mechanism of cooling remains relatively obscure. Consequently, it is not known whether the current cryogen delivery devices are optimized with respect to cooling efficiency and localization of cooling. The only type of cryogen delivery device that has thus far been studied in a medical context is a fuel injector valve without delivery nozzle [7,8].

In this paper, we investigate how changes in nozzle design influence the cooling characteristics of a cryogen spray. An existing method to quantify these characteristics is analyzed and a new one is introduced. Finally, we hypothesize on why sprays from wider nozzles appear to extract heat faster than sprays from narrow nozzles.

*Correspondence: 1002 Health Sciences Rd. East, Irvine; e-mail: wverkru@bli.uci.edu, fax: +1-949-824-6969

2. Methods

2.1. Cryogen delivery

The cryogen that we used (1,1,1,2 tetrafluoroethane, also known as R134a) is the same as that used in current clinical devices and in previous studies. It has a boiling temperature of –26 °C and is kept in a steel canister at 25 °C at which the saturation pressure of the cryogen is approximately 6.6 bar. An electronically controlled automobile fuel injector is attached to the canister.

We have designed and produced four different nozzles (Figure 1). Each consists of a copper body, which fits tightly around the valve body and holds a stainless steel tube of length L and inner diameter D (Table 1). All values for L and D were chosen arbitrarily except for the inner diameter of 0.69 mm, which is similar to that of a commercially available cryogen atomizer (Candela? , DCD for ScleroPlus?).

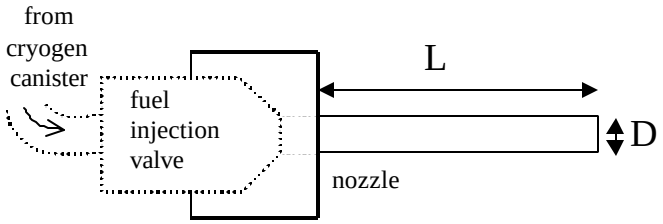

Figure 1: Sketch of the fuel injector (dashed lines) and nozzle (solid lines).

Table 1: Length L and inner diameter D of the four nozzles used in this study.

Nozzle	L (mm)	D (mm)
Short Narrow (SN)	31.75	0.69
Short Wide (SW)	31.75	1.37
Long Narrow (LN)	63.5	0.69
Long Wide (LW)	63.5	1.37

2.2. Fast Flashlamp Photography (FFLP)

A progressive scan digital camera with a shutter speed of 60 ?s (Pulnix, Sunnyvale, CA) was triggered in synchronicity with a flashlamp (EG&G electronics, Salem, MA). The flashlamp provides illumination gating by 2-5 ?s long pulses that "freeze" the image of flying cryogen droplets. The supporting electronics enable acquisition of image sequences at 30 frames per second or individual images at precisely controlled delays with respect to the cryogen spurt.

We photographed either the spray shape or a cryogen sprayed block during and after the spurt. To obtain the spray shape photographs at low magnification, the nozzle, the flashlamp, and the camera, were all positioned in the same horizontal plane. The camera was placed perpendicular to the nozzle while the flashlamp was positioned at a 30? angle from the camera, directed towards the nozzle tip. For the photographs of the cryogen sprayed block, the camera was oriented perpendicular to the spray block and the flashlamp was placed at a 45? angle from the camera. The axis of the cryogen spray was at an angle of approximately 20 ? with the normal to the block.

2.3. The cooling model.

For the mathematical description of CSC, we use the 1-D heat diffusion equation (1) with the Robin boundary condition (2) as proposed by Anvari et al. [7]. As a first order approximation, it describes temperatures $T(z,t)$ at time t and depth z in a cryogen sprayed object reasonably well [8].

$$?^2T(z,t)/?z^2 \; ? \; (?c/?)?T(z,t)/?t \tag{1}$$

$$? \left(?T(z,t)/?z \right)\Big|_{z?0} \; ? \; h_{cryo} \left(T(0,t) ? T_{cryo} \right) \tag{2}$$

Parameters ? , ? and c are the thermal conductivity, density and specific heat of the sprayed object, respectively. T_{cryo} is the temperature of the cryogen droplets when they arrive at the object. The heat transfer coefficient h_{cryo} is a measure of the quality of thermal contact between the cryogen droplets and the object.

Ideally, cooling of skin should only cool the superficial layers (epidermis and basal layer) while keeping the temperatures of the deeper layers (where the target chromophores such as blood vessels or hair follicles are), intact. Inevitably, however,

thermal diffusion (equation 2), induces some cooling at greater depths. How much these deeper layers are cooled depends strongly on the parameter h_{cryo} as illustrated in the following paragraph.

We assume that temperature difference between basal layer and a deeper target (Figure 2a) is a good measure for spatial cooling selectivity [9, 10]. In Figure 2b this difference is plotted as a function of time during a cryogen spurt, for a basal layer at a depth of 60 ?m and a target at 300 ?m. Each curve is the result for a different h_{cryo} value (as indicated in the graph), while T_{cryo} = - 44 °C for all curves. The curves were obtained by numerically solving equations (1) and (2) for the skin model illustrated in Figure 2a. Thermal properties for epidermis and dermis were as used in Sturesson and Andersson-Engels [9], and we assumed optimal thermal contact at the epidermal dermal junction.

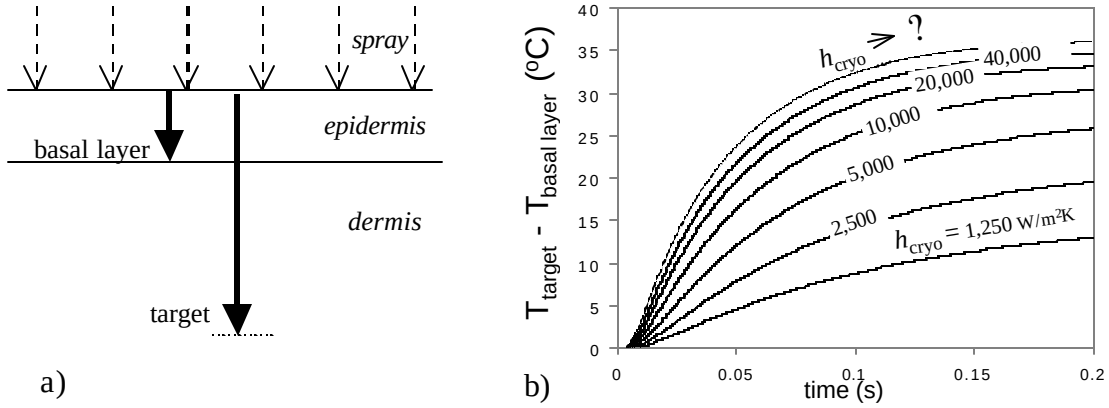

Figure 2: a) Simple 1-dimensional skin model illustrating the positions of the basal layer and a dermal target. b) During a cryogen spurt, the basal layer cools faster than the target (at a depth of 300 ?m). For small values of h_{cryo}, the heat extraction at the surface is slower and, therefore, cooling selectivity is lower.

The curves in Figure 2b illustrate how the cooling selectivity strongly depends on the value of h_{cryo}. For low h_{cryo} values, relatively small temperature differences are achieved. For large values, considerably larger spatial temperature differences are obtained and the effect of CSC is predicted to be more beneficial.

2.4. Epoxy-block / dynamical method

Torres et al. [8] showed that an epoxy-block with embedded thermocouples can be used to estimate h_{cryo} and T_{cryo}. We use the same method with a slightly different design of the block. Using a silicon mold, we cast a solid epoxy-block (medium viscosity, RBC Industries, Warwick, RI) on which we attached type E thermocouples (90 ?m diameter), using liquid epoxy as a glue. After the glue had hardened, we cast another layer of epoxy on top of this. After this layer had hardened for at least 24 hours, we carefully sanded it down until it was about 100 ?m thick and again glued thermocouples.

By repeating the procedure of gluing thermocouples and casting an additional layer of epoxy on top of the previous one, we obtained an epoxy-block with thermocouples embedded at depths of 55, 91 and 251 ?m. We used a microscope (40x) as a depth measuring device in epoxy with an accuracy of approximately 5 to 10 ?m, depending on depth of the thermocouples. We 'calibrated' the microscope by focussing on both sides of a thin epoxy layer of known thickness and measured the translation of the objective. Before we cast the last layer of epoxy, we applied an array of thermocouples to investigate possible lateral features of the CSC. These thermocouples were 1 to 2 mm apart from each other, while their depths ranged from 60 to 150 ?m. During an experiment, the spray axis was always along the line of the axially distributed thermocouples (see Figure 3a). For data acquisition, a standard A/D converter board (instruNet, Omega Engineering Inc. Stamford CT) was used.

2.5. Metal rod / steady-state method

In the alternative set-up (Figure 3b) we used a copper (copper alloy 110) rod with radius R = 3.18 mm (1/8``) as the primary material to be cooled. We have two main reasons for choosing copper. First, this material has a high thermal conductivity (391 $Wm^{-1}K^{-1}$), more than three orders of magnitude higher than that of epoxy (on the order of 0.2 $Wm^{-1}K^{-1}$). Second, its thermal properties are known with high accuracy.

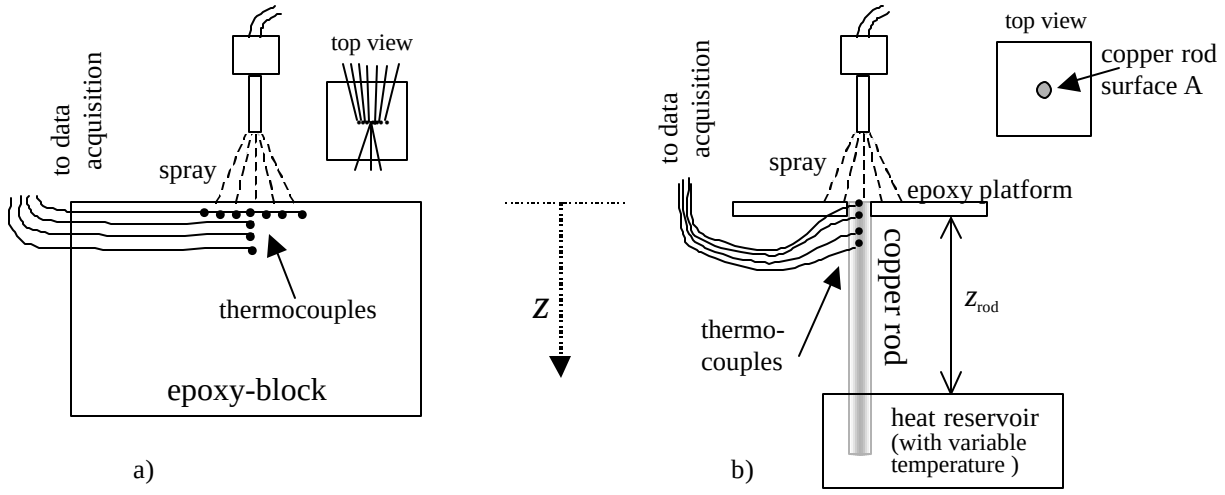

Figure 3: Cross-sectional views of setups for the epoxy-block (a) and metal rod (b) methods. The insets show the top views. The epoxy-block uses a dynamical model whereas the metal rod setup is based on steady state temperature measurements. The heat reservoir can be anything that 'pins' the metal rod at position $z = z_{rod}$ at fixed temperature.

The much higher conductivity of copper 'explodes' the scale of the problem which makes the exact location of the thermocouples much less critical for the estimate of h_{cryo}. However, when using equations (1) and (2), we implicitly assume that the sprayed area (on the order of 1 cm^2), is much larger than the diffusion length in the sprayed material during the measurement (< 1mm for epoxy). Using a metal, which has much larger diffusivity and, therefore, also much larger diffusion length, the spray ought to be magnified as well in order to maintain the one-dimensionality approximation. Instead, we chose to maintain the validity of this approximation by using a rod geometry (cross-sectional area A). The top of the rod is surrounded by an epoxy platform, which is a good thermal insulator compared to copper. This platform prevents cryogen from dripping along the rod, ensuring that the heat current on the top of the copper rod is primarily along the axis of the rod. For the same reason, we insulated the sides of the copper rod.

An additional major change in the new method is that we measure temperature profiles in a steady state mode instead of dynamically as in the epoxy-block method. Cryogen is sprayed on the top of the rod (and the epoxy platform) while heat power H is being supplied at the bottom of the rod. The heat supply can be anything providing heat: e.g. a water bath or a soldering iron with variable power attached to the rod. (Figure 3b).In our preliminary experiment we used a hair dryer, blowing hot air at a distance z_{rod} from the sprayed surface. After a period of several thermal relaxation times ?of the metal rod, the temperature profile in the metal rod has stabilized such that the heat extraction at the sprayed surface equals the heat supply H. The thermal relaxation time can be estimated as $? = z_{rod}^2/?$ where ??is thermal diffusivity of copper (1.12 10^{-4} m^2/s). In our experiment z_{rod} was approximately 10 cm, which corresponds to ?? 90 seconds.

Once the steady state mode is reached, the boundary condition and temperature $T(z)$ in the rod can be expressed with equations (3) and (4) respectively.

$$? [?T / ?z] \quad ? \quad h_{cryo}[T(z ? 0) ? T_{cryo}] \quad ? \quad H / A \tag{3}$$

$$T(z) \quad ? \quad T(z ? 0) ? z [?T / ?z] \tag{4}$$

The gradient $?T/dz$ which is constant along the entire length of the rod, can be measured relatively accurately with thermocouples attached to the side of the rod (Figure 3b). The temperature at the sprayed surface of the metal rod $T(z=0)$ can be determined by extrapolating the temperature profile $T(z)$ to $z = 0$ using equation (4). Next, we rewrite and generalize equation 3 to:

$$?T / ?z?_x ? (h_{cryo} / ?)[T_x(z ? 0) ? T_{cryo}] \tag{5}$$

where x is an index for a steady state measurement taken with a variable heat supply H_x. If we perform a series of steady state measurements for a number of different heat powers H_x, and plot the gradients $[?T / ?z]_x$ as a function of their corresponding surface temperatures $T_x(z=0)$, we expect the points to lie on a straight line. The slope of this line represents

(h_{cryo}/?), while the intersection with the horizontal axis gives the estimate for T_{cryo}. Obviously, it is implicitly assumed that T_{cryo} and h_{cryo} are constant within the range of surface temperatures involved.

3. Results

3.1. Fast Flashlamp Photography

Figure 4 shows the shapes of sprays produced by two different nozzles: long/wide (LW) and long/narrow (LN). Cryogen exits the LW nozzle in a jet-like fashion, while the narrow one appears to induce a much finer atomization of cryogen. The different type of atomization is clear, in particular near the nozzle tips (indicated by arrows). Figures 4c and 4d show that at 6 cm distance from the nozzle tips, the diameter of spray from LN (d) is still wider than that from the wider nozzle LW (c).

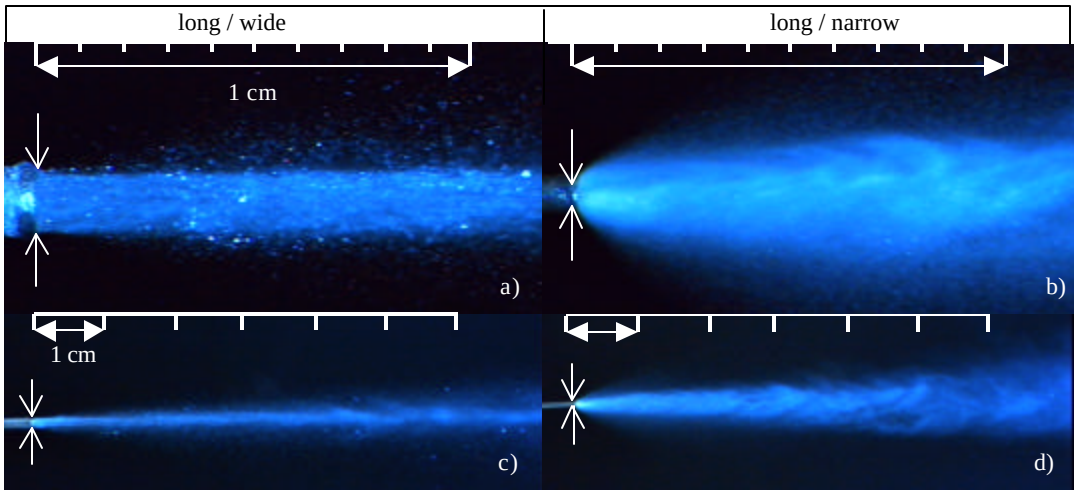

Figure 4: Photographs of cryogen ejected by a long wide (a and c) and long narrow (b and d) nozzle at high (a and b) and low (c and d) magnifications (see scales at top of Figures). The arrows indicate position and the inner diameter of the nozzle tip.

The same difference between narrow and wide nozzles (more atomization and larger cone angle of spray with narrow nozzle), was also found for the shorter nozzles SN and SW, although somewhat less pronounced than for the long nozzles. When comparing the nozzles SW with LW, and SN with LN, we found that the shorter nozzles produced slightly more atomization, and correspondingly larger cone angles, than the longer ones.

Figure 5a shows that 30 ms after the end of a spurt from a long wide nozzle, the sprayed area is dry, while a cryogen pool persists outside the sprayed area. For the narrow nozzle (Fig. 5b), the sprayed area is covered with an oblique cryogen pool. This pool is surrounded by a ring of snow/frost, while the area outside this ring is dry.

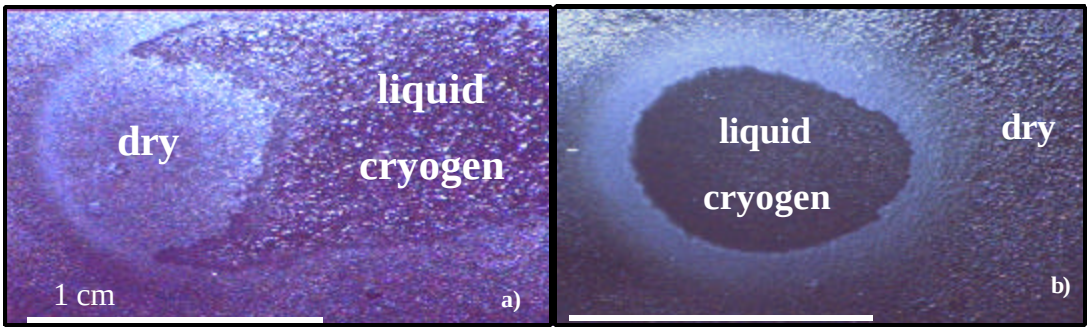

Figures 5: Photographs of a cryogen sprayed block taken 30 ms after the end of a 20 ms spurt from a LW (a) and LN (b) nozzle. Cryogen was sprayed from the left at an angle of about 20 degrees normal to the block. The bars represent a length of 1 cm. The area sprayed with the wide nozzle is dry. When sprayed with the narrow nozzle, a cryogen pool persists on the sprayed area.

3.2. Epoxy-block / dynamical method.

In addition to photographic investigation of the sprays, we tried to estimate the heat extraction coefficient for each nozzle. For the calculation of the temperature curves, we took into account a thermocouple response time of 9 ms. Values used for the thermal properties are ? ????????kg m^{-3}, c = 1,200 Jkg^{-1}K^{-1} and ? = 0.14 Wm^{-1}K^{-1}. The value for the specific heat is approximately equal to the average of the values as measured by different groups and the value for conductivity is measured for epoxy at 0 °C. In Figure 6, temperatures measured for the short wide nozzle are shown. A reasonable fit was found with T_{cryo} = -49 °C and h_{cryo} = 10,000 Wm^{-2} K^{-1}.

We found that the predicted curves are not very sensitive for the value of h_{cryo}. We used the curve corresponding to –49 °C and h_{cryo} = 10,000 Wm^{-2} K^{-1} as a 'central curve' to investigate the range of h_{cryo} corresponding to curves that deviate from the central curve by not more than 0.5 °C. Within estimated uncertainties in the depth of the thermocouples (? 5 ?m) and T_{cryo} (? 1 °C), we found a range of h_{cryo} = 5,900 to 30,000 Wm^{-2} K^{-1}. The central curve as well as the curves corresponding to the extremes for h_{cryo} are plotted in Figure 6.

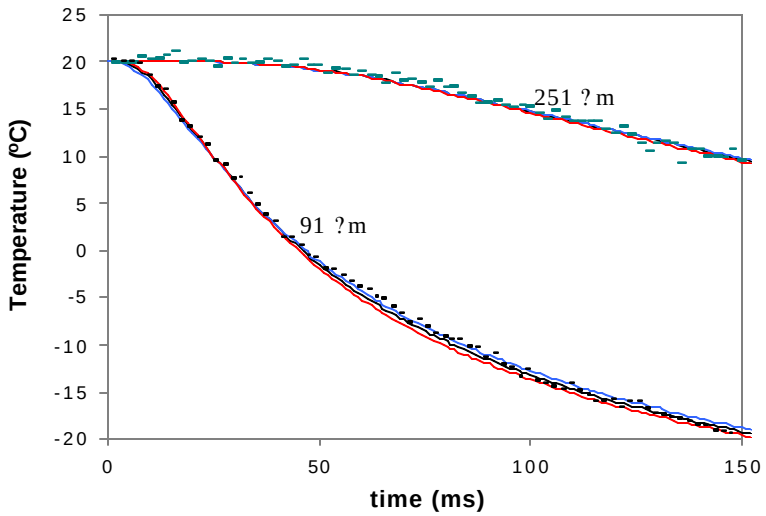

Figure 6: Measured (symbols) and calculated (lines) temperatures for thermocouples at depths indicated. Values of 10,000 Wm^{-2} K^{-1} for h_{cryo} and –49 °C for T_{cryo} fit the data very well. Allowing some uncertainty in depths of the thermocouples and T_{cryo} we found that h_{cryo} values between 5,900 and 30,000 Wm^{-2} K^{-1} deviate from the central curve by not more than 0.5 °C (see text). The predicted curves for the 251 ?m deep thermocouples are indistinguishable.

From the values of 5,900, 10,000 and 30,000 Wm^{-2} K^{-1}, we conclude that the margin of error for h_{cryo} is strongly skewed in the positive direction. This is due to the fact that temperature profiles depend relatively weakly on h_{cryo} when h_{cryo} is large (Figure 2b). Measurements of cryogen deposition with smaller h_{cryo} are expected to have a smaller margin of error. A similar investigation of h_{cryo} shows that, with the same error margins, h_{cryo} only varies from 1,860 to 3,800 Wm^{-2} K^{-1} around a central value of 2,500 Wm^{-2} K^{-1}.

Due to the relatively large margin of error in the estimate of h_{cryo}, the epoxy-block is of limited use quantitatively. As a means to compare the heat extraction for the different nozzles in a qualitative way, however, it can be very useful. Figure 7a shows temperatures in a thermocouple during a spurt from nozzle LN or LW. The sprays were aimed such that the thermocouple was in the center of the spray. The wide nozzle induces a significantly faster cooling than the narrow nozzle. During the first 30 ms of the spurt, nozzle LW cools only slightly more than the narrow nozzle. Then, nozzle LW cools significantly faster than nozzle LN. Considering equation 2, the faster cooling can be explained by either a higher value for h_{cryo} or a lower value for T_{cryo}. In Figure 7b, showing the same curves as in 7a on a different time scale, the curves cross at approximately t = 1.2 s. For longer times the temperatures for LN continue to decrease faster than those for LW. Assuming that the temperatures at greater t approach the value of T_{cryo} for each nozzle, we can conclude that the initial faster cooling of nozzle LW *must* be due to a higher value for h_{cryo} because it can not be explained by a lower value for T_{cryo}. We found very similar results when comparing nozzle SW with SN.

Figure 7c shows temperatures during the same spurts as for Figure 7a, now measured in a thermocouple at 3mm radial distance from the spray center. Similarly to curves in Figure 7a, the cooling is significantly faster for nozzle LW compared to nozzle LN. Temperatures at the periphery were very similar to those in the center of the spray when nozzle LW was used. For the narrow nozzle, the temperature evolution at 3 mm from the center was considerably different from that in the center. An initial slow temperature decrease was followed by a faster decrease, starting around t = 0.04 s. Considering the relatively small standard deviation in the signals we conclude that this feature is significant. Moreover, we observed very similar features in a peripheral thermocouple on the other side of the spray center.

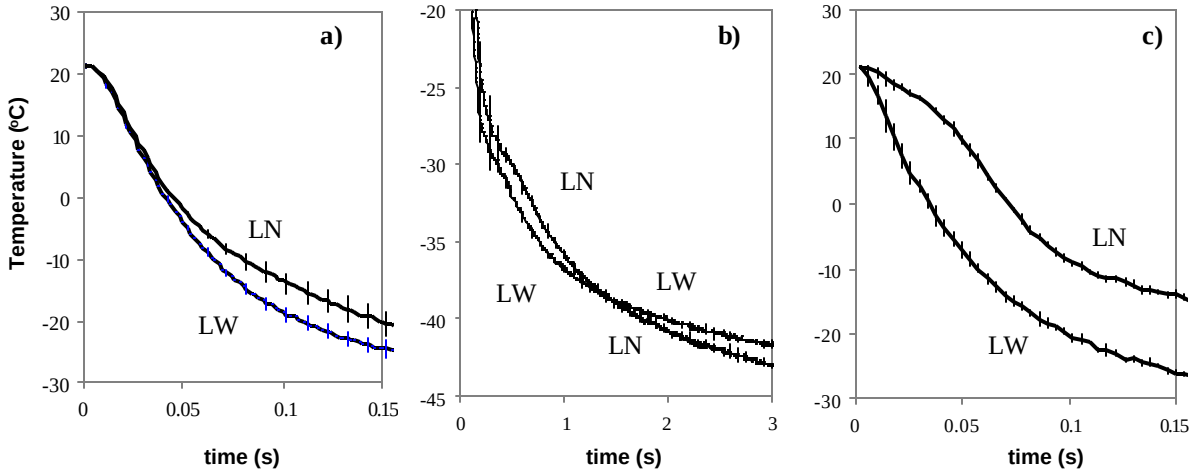

Figure 7: Temperature in a 90 ?m deep thermocouple during cryogen spurts from a long narrow (LN) and long wide (LW) nozzle in the center of the spray at small time scale (a) and larger time scale (b). In c) temperatures at 3 mm radial distance from the spray center for the same spurts as in a) and b). The lower temperatures for the narrow nozzle at large *t*, suggest that the cryogen droplet temperature T_{cryo} is lower than for the wider nozzle. Each curve is the averaged temperature from 8 spurts. Error bars indicate standard deviations.

Whereas the model reasonably fits temperatures measured when using the wide nozzles, this is not the case for the narrow nozzles. This is particularly true for the temperatures measured in the periphery of the sprayed spot (Figure 7c) but even in the center (Figure 7a) it was not possible to fit the curves satisfactorily. This suggests that for these curves, the Robin boundary condition with constant h_{cryo} and T_{cryo} is not a good model.

3.3. Metal rod / steady state method.

To illustrate the steady state method for estimation of h_{cryo} and T_{cryo}, we present preliminary results for the nozzle SW. In Figure 8a, we show temperature evolutions, measured with four thermocouples at distances of 0.5, 9.5, 15 and 30 mm from the sprayed surface.

By repositioning the hair dryer, thus changing the heat supply to the rod, we induced four steady state temperature gradients in the rod (around t = 250, 450, 725 and 1100 s) which are illustrated in Figure 8a. At t =300 and 850 s we saw that the temperature gradient changed very slowly and decided to change the heat supply somewhat more. At t = 1150 we stopped cooling, resulting in all temperatures to rise quickly. In Figure 8b we plotted the temperatures in the four thermocouples as a function of their position along the rod, for times t as indicated by the vertical lines in Figure 8a.

We performed linear regression fits on the data in Figure 8b and plotted the resulting temperature gradients (ranging from 0.64 to 1.06 K/mm) as a function of the corresponding surface temperatures T(z=0) (ranging from –39 to –36 °C). Finally, a linear fit of this set of data gives estimates for h_{cryo} and T_{cryo} according to equation 5. To explore the margin of error, we plot the steepest and shallowest curves, possible within error bars. This analysis results in h_{cryo} = 77,000 and 46,000 $\mathrm{Wm^{-2}\,K^{-1}}$ with corresponding T_{cryo} values of - 42.3 and - 45.0 °C. respectively.

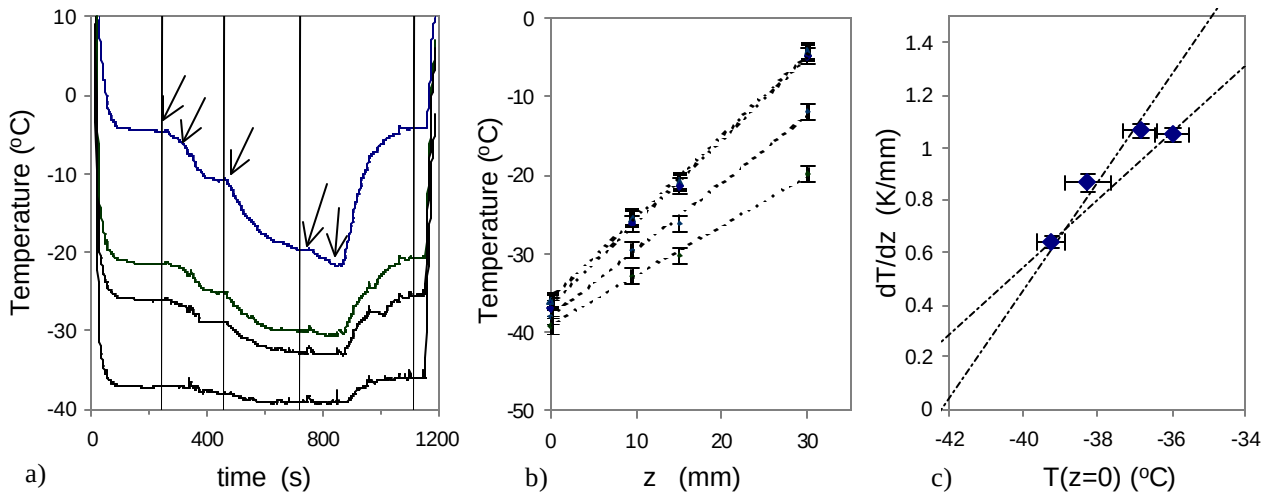

Figure 8: a) Temperature evolutions as measured by four thermocouples positioned at z = 0.5, 9.5, 15 and 30 mm from the sprayed end of the copper rod. The vertical lines indicate the times for which the temperatures are plotted versus thermocouple position z in b). The arrows indicate moments at which the heat supply was changed. The lines in Figure b are linear fits while the error bars represent estimated measurement errors. In c), the temperature gradients of the linear fits in Figure b) are plotted (symbols) versus the corresponding surface temperature T(z=0) with error bars representing standard error (95% confidence interval). The dashed lines correspond to h_{cryo} = 77,000 and 46,000 $Wm^{-2} K^{-1}$ for the steepest and shallowest curves respectively. Corresponding values for T_{cryo} are –42.3 and –45 °C

4. Discussion

4.1. Uncertainty in the determination of h_{cryo} and T_{cryo} with the epoxy-block method

As mentioned in the results section, we found that there was a considerable range of values for h_{cryo} and T_{cryo} that would reasonably fit the measured curves within experimental error using the epoxy-block method. Here, we would like to list a number of factors that contribute to the uncertainty in the estimated values for h_{cryo}:

1. Depth and size of thermocouples,

2. Estimate of T_{cryo},

3. Onset of the spray,

4. Thermal properties of the epoxy,

5. Perturbation of temperature field due to thermocouples,

6. T_{cryo}, and h_{cryo} in particular, may vary during the spurt, and

7. The spray may be laterally inhomogeneous.

1) The thermocouple's depths can be established within an accuracy of about 5 ?m for the shallow, and 10 ?m for the deeper thermocouples. This is a relatively large error, given the depth of the shallowest thermocouples of only several tens of ?m, and the large sensitivity of the $T(t)$ curves for small changes in depth. Also the size of thermocouples should be considered as a possible source of experimental error. Only when the temperature gradient over the dimension of the thermocouple bead is constant, the thermocouple may measure the average temperature and its effective measuring depth is its central depth. Considering the strong temperature gradient near the surface, it is not clear what the effective measuring depth of the thermocouple is [11]. In particular when the temperature gradient is not constant, (which is the case during a cryogen spurt, neither in space, nor in time) the effective depth is difficult to estimate and may even change during the spurt.

2) We consider two ways to estimate the value of T_{cryo}. First, using a thermocouple placed on the surface of the epoxy-block [8], or, second, the asymptotic temperature of the superficial embedded thermocouples for very large long spurt durations (several seconds). When using the first method, the thermocouple may measure an averaged temperature in a cryogen layer, in which a temperature gradient may exist. Or, if the cryogen layer is smaller than the dimension of the thermocouple bead,

the temperature may be an average of that of air and liquid cryogen. Apart from this consideration, noise in this signal introduces a measuring error of approximately 1 ?Celsius. Using the second method to estimate T_{cryo}, as we did in this study, snow or ice forms on the surface during long spurts. This may invalidate the assumption that the asymptotic temperature value is a good indicator for T_{cryo}. Wiping away the snow may partly revalidate the assumption.

3) By monitoring the input signal to the injector valve simultaneously with the signal from a thermocouple positioned in the center of the cryogen spray, we found that the first cryogen droplets appear 3 to 6 ms after the onset of the input signal. This means that the actual onset of the spurt on the epoxy-block (defining t=0) can not be assessed from the electronic input signal to the valve. Therefore, it must be assessed from the first decrease in temperature of the most superficial thermocouple.

4) In our experience, it has been difficult to establish consistent thermal properties for our epoxy. Measurements by three different groups on samples of the same epoxy (same cast, samples studied originated from a volume several mm^3 large), resulted in relatively large variations of up to 20% in the diffusivity. Moreover, all groups reported a decrease of specific heat by 16% to 40% (depending on the group) when cooling from room temperature down to –50 °C. Each of the groups was using appropriate methods to measure the thermal properties: differential scanning calorimeters for specific heat and the 'flash method' for thermal diffusivity (ASTM procedure E1461). In the estimate of the margin of error as used in the methods section (Figure 6) we only considered the experimental errors as listed by points 1 to 3. It is important to realize that, when fitting the model to measurements, the actual parameter that is estimated is the reduced heat transfer coefficient $h_{cryo}/?$, rather than $h_{cryo.}$ Therefore, it is easy to see that an uncertainty in the conductivity adds to the uncertainty in the estimate of h_{cryo}.

5) When non-insulated thermocouple wires are used, and the thermal conductivity of the wires is much higher than the embedding medium, the presence of the thermocouple can influence the temperature distribution [11]. In particular when a strong temperature gradient exists along the thermocouple wires, the perturbation of the temperature field around the thermocouple can be significant. Quantification of these errors is very complex. In our epoxy-block, thermocouple wires were positioned parallel to the surface, which helps to minimize this effect.

6) Equations (1) and (2) assume that both h_{cryo} and T_{cryo} are constant during the spurt. Figures 7a to 7c indicate that, for the nozzle LN in particular, this is probably not the case. Since the model can not account for relatively sudden changes in cooling rate because the measured temperature curves can not be satisfactorily fitted with the model; and

7) Cryogen droplet temperature, size, density and speed may vary laterally in the spray.

Points 5 to 7 are difficult to quantify in terms of a margin of error. However, they may help to remind that equations 1 and 2 provide a first order approximation to the problem only.

4.2. metal rod / steady state method

With the steady state method we estimated the h_{cryo} value for nozzle SW to be between 46,000 and 77,000 $Wm^{-2} K^{-1}$, while T_{cryo} was estimated to be –43.6 ? 1.5 °C. These values are estimates for the spray on a relatively smooth object with a surface temperature of approximately –36 °C. Our estimate of h_{cryo} for nozzle SW is 60,000 ? 15,000 $Wm^{-2} K^{-1}$. Typical values of the heat transfer coefficient for forced convection of liquids range from 50 to 20,000 $Wm^{-2} K^{-1}$ while for convection with a phase change a typical range is 2,500 – 100,000 $Wm^{-2} K^{-1}$ [12]. We think these high values may indeed be realistic estimates for this nozzle. Despite the fact that the surface temperature of –35 °C is below the cryogen boiling temperature (-26 °C), vaporization still takes place because the local pressure is far below the vapor pressure at the local temperature.

We have not investigated all possible sources of error with this method. However, a first estimate of the margin of error suggests that the accuracy of the estimates for h_{cryo} is surprisingly high; in particular when considering the small sensitivity of temperatures for h_{cryo} around h_{cryo} = 60,000 (see Figure 2b). Using a hair dryer as a heat source, we were able to establish steady state surface temperatures of –39 to –35 °C. Because the estimate of h_{cryo} becomes more accurate for a larger range of T(z=0) (see Figure 8c), we expect to estimate h_{cryo} and T_{cryo} with higher accuracy when using more powerful heat sources such as a soldering iron or a heat gun.

The steady state method is not suitable for the estimation of the average cooling characteristics of a short spurt, e.g. 100 ms. Therefore, it is important to note that the value of 65,000 ? 15,000 $Wm^{-2} K^{-1}$ is not to be compared directly with for h_{cryo} estimates from epoxy-block measurements. Even if h_{cryo} can be estimated very accurately with either method, the value may be not applicable for the same cryogen spray on skin. Skin surface is much less smooth than epoxy or the surface of the metal rod. Moreover, it has been suggested that cryogen cooled skin may involve storage of latent energy during freezing of skin [13] which would change thermal dynamics within skin as well as on the surface.

In future experiments, we intend to reduce the diameter of the rod and scan laterally, as well as axially through the cryogen spray, to acquire a better understanding of atomizing characteristics of different nozzles. In another study [14], we describe a model for cryogen droplet temperature as a function of distance from the nozzle tip. In the present study we used data for T_{cryo} as measured with the epoxy-block. Another advantage of the steady state method is that it enables us to study heat transfer mechanisms of CSC when spraying objects at a constant surface temperature. For example, we plan to study whether h_{cryo} is different for surface temperatures above -26.1 °C (cryogen boiling temperature) than for surface temperatures below -26 °C.

4.3. Comparison of the nozzles and cryogen deposit mechanisms

The diameter of the nozzles was more critical than their length for the shape and cooling efficiency of the sprays. The narrow nozzles ejected the cryogen in a spray with a relatively large cone angle and appeared to atomize the cryogen in relatively small droplets. The wider nozzles, on the contrary, produced a jet rather than a spray. Cryogen droplets from the jet-like spray, seem to impinge on accumulated cryogen with enough kinetic energy to pierce through the cryogen layer. Thereby, these droplets are in much better thermal contact with the object than the finer droplets from the narrow nozzles.

The only significant difference we found between long and short nozzles was that the shorter nozzles seemed to eject more cryogen than the longer nozzles. We derived this from the fact that after equal spurt durations, a cryogen pool remained on the sprayed block for a longer time with the short nozzles.

Although we did not quantify cooling characteristics of the narrow nozzles, the heat transfer coefficient is definitely lower than for the jet-like sprays from the wide nozzles (Figures 7a and 7b). In terms of spatial selectivity of cooling, the premise of CSC, the wider nozzles are preferable. However, with the nozzles investigated in this study, the jet-like spray seems to be accompanied by a poor localization of the cooled area. Moreover, clinically, the more violent impact of the larger, and possibly faster, droplets on skin is considerably more uncomfortable than the more gentle impact of finer atomized (and better localized) spray. It is important, therefore, to quantify the cooling characteristics of the narrow nozzles more accurately. It should be noted that the dependence of the cooling selectivity on h_{cryo} is strongly non-linear (Figure 2b). For example, a small variation in h_{cryo} around 2,500 $Wm^{-2} K^{-1}$ is predicted to have a much greater effect on the expected cooling selectivity than a similar relative change around h_{cryo} = 20,000 $Wm^{-2} K^{-1}$. For h_{cryo} values of approximately 10,000 $Wm^{-2} K^{-1}$ or more near optimal cooling selectivity is achieved, and a further improvement of h_{cryo} is of marginal value. If a value for h_{cryo} is measured at 2,500 $Wm^{-2} K^{-1}$, however, considerable room for improvement exists. If, in future measurements, the h_{cryo} value for narrow nozzles is sufficiently large (> 10,000 $Wm^{-2} K^{-1}$), better localization and more comfortable impact of the spray would probably be preferred over narrow nozzles with higher h_{cryo}. If the value is much lower, however, one may have to trade off good spatial cooling selectivity against a good surface localization and patient comfort.

Our observations suggest that a layer of accumulated cryogen exists on the sprayed object during the spurt. This cryogen layer is cooled at the top through vaporization, and heated on the bottom by the object. Considering the relatively low thermal conductivity for cryogen R134a (0.0824 $Wm^{-1}K^{-1}$), the cryogen layer may act as a relatively good thermal barrier between the cold droplets and the relatively hot object [15].

The kinetic energy of the smaller droplets is not sufficient to break through the cryogen layer and simply coalesce with it (Figures 9a to 9c). The movement of the cryogen is basically one-dimensional. In contrast, the droplets ejected by the wider nozzles have a much larger kinetic energy due to their larger mass and possibly also a greater velocity. Therefore, it is likely that the cold cryogen droplets displace the relatively warm cryogen layer and come in close contact with the object surface (Figures 9d to 9f). Such a violent impact is associated with a strong convection of cryogen towards the periphery of the sprayed spot. Even if the droplets do not pierce through the layer entirely, the enhanced convection may improve heat transfer from object to cryogen droplets.

Photos of the cryogen impact, when using the wider nozzles, show that in the center of the sprayed spot, the cryogen layer disappears very quickly following the end of the spurt (Figure 5a) whereas for the narrow nozzles cryogen remains present much longer (Figure 5b). Nozzle LW produced a cryogen pool to the right of the spot of impingement while the cryogen at this spot itself has evaporated already (the relatively bright, circular spot in the left part of Figure 5a). The quick disappearance of the cryogen pool for the nozzles LW suggests that the cryogen layer is much thinner than the cryogen pool for nozzle LN. Nozzle LN, under similar conditions, produced a cryogen pool (dark elliptical area in the center of Figure 5b), more or less at the spot of impingement. The fact that this pool remained there for considerable time may suggest that the layer of cryogen is much thicker for this nozzle. The circle of frost around the cryogen pool, was observed for the narrow nozzles only.

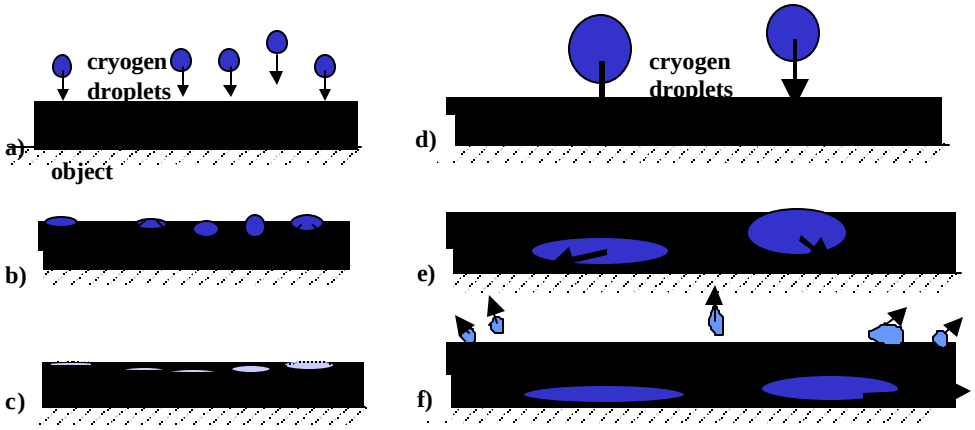

Figure 9: In a) to c) we have sketched three different stages of how the relatively small droplets may impinge on the cryogen layer and the object (e.g. epoxy or skin). Figures d) to f) sketch the different stages of how the larger droplets of a jet may pierce through the layer and eventually be in direct thermal contact with the object.

We believe that the thinner cryogen layer on the sprayed spot during the spurt from a wide nozzle is mainly due to two phenomena. First, the larger droplets have a greater kinetic energy due to their larger mass and perhaps also larger velocity. Their impact on the cryogen layer is strong enough to cause some cryogen to splash back from the object (indicated in 9f)) which results obviously in less cryogen on the objects' surface. We have observed this splashing, using FFLP, with the wider nozzles only. Secondly, more jet-like cryogen spray from the wider nozzles results in a strong flow of cryogen directed from the center of the sprayed spot towards the periphery (Figure 5a).

Thermocouples, positioned approximately 3 mm from the spray axis, show characteristically different temperature evolutions than thermocouples in the center of the spray. This suggests that the relevant spray characteristics (T_{cryo} and h_{cryo}) are not the same throughout the entire sprayed spot, (point 7 in section 4.1). We can speculate on possible reasons for the lateral inhomogeneity. In the center of the spray, the cooling by the narrow nozzle is similar to that by the wide nozzle during the first 40 ms. Possibly, these 40 ms represent the time it takes to build up a cryogen or ice/snow layer that starts acting as a thermal barrier after the 40 ms have elapsed. The features in the signal for the narrow nozzle at the periphery are more complex. We are currently setting up a phase Doppler particle analyzer (PDPA) system which will measure droplet size, density and velocity distributions at any point in the spray. This will probably help to explain lateral differences in the sprayed area as well.

5. Conclusions

The nozzles with wide diameter deposit cryogen in a jet like fashion (large, fast moving droplets) and cool the sprayed object faster (larger heat transfer coefficient) than those which atomize the cryogen in a spray with relatively small and slow moving droplets (nozzles with narrow diameter). This is probably due to the ability of fast and large droplets to pierce through a cryogen layer which enables them to be in relatively good thermal contact with the sprayed object.

A relatively large margin of error exists for the estimate of h_{cryo} when using realistic experimental errors in the fitting procedure. The sensitivity of h_{cryo} to experimental error is much larger if the central value of h_{cryo} is large.

Measurements with the epoxy-block show that h_{cryo} and T_{cryo} vary laterally as well as temporally for sprays produced by the narrow nozzles. Due to these variations, we were not able to satisfactorily fit the model to the measured temperatures. For the wide nozzle we were able to fit measured temperature curves with h_{cryo} values from 5,900 to 30,000 $\mathrm{Wm^{-2}\,K^{-1}}$. Even the lower estimate is considerably larger than the value of 2,400 $\mathrm{Wm^{-2}\,K^{-1}}$ reported for a fuel injector without a nozzle [8].

We have developed and tested an alternative method to estimate h_{cryo} and T_{cryo} for CSC. With this method we found an h_{cryo} value of 60,000 ? 15,000 $\mathrm{Wm^{-2}\,K^{-1}}$ for a surface temperature around –37 °C. T_{cryo} was estimated as –44 ? 1.5 ° C. With this method it will be possible to analyze h_{cryo} for a range of different locations in the sprayed area. It also allows us to investigate whether h_{cryo} is constant during a spurt or whether it depends on surface temperature and therefore changes during the spurt.

Acknowledgment

This work was supported by a research grant from the Institute of Arthritis and Musculoskeletal and Skin Diseases (AR43419) at the National Institutes of Health (to JSN), Candela Corporation and by the Slovenian Ministry of Science and Technology (BM). Institutional support from the Office of Naval Research, Department of Energy, National Institutes of Health, and the Beckman Laser Institute and Medical Clinic Endowment is also acknowledged. Discussions with Karl Pope and Prof. Lavernia on the physical and clinical aspects of CSC are greatly appreciated. We thank Matja` Krajnc and Ida Poljan{ek of the University of Ljubljana and Steven Dallek of the Naval Surface Warfare Center, Maryland for measurements of thermal properties. Emily Williams' and Adrian Prokop's help with the experiments are greatly appreciated.

References

1 A.J. Welch, M. Motamedi, and, A. Gonzalez. "Evaluation of cooling techniques for the protection of the epidermis during Nd:YAG laser irradiation of the skin". In: Nd-YAG Laser in Medicine and Surgery. New York: Elsevier, 1983.

2 J.S. Nelson, T.E. Milner, B. Anvari, B.S. Tanenbaum, S. Kimel, L.O. Svaasand, and S.L. Jacques: "Dynamic epidermal cooling during pulsed laser treatment of port-wine stain. A new methodology with preliminary clinical evaluation". *Arch Dermatol*, 131(6):695-700, 1995.

3 H.A. Waldorf, T.S. Alster, K. McMillan, A.N. Kauvar, R.G. Geronemus, and J.S. Nelson. "Effect of dynamic cooling on 585-nm pulsed dye laser treatment of port-wine stain birthmarks". *Dermatol Surg*; 23:657-62, 1997

4 E.J. Fiskerstrand, L.T. Norvang, and L.O. Svaasand. "Laser treatment of port wine stains; reduced pain and shorter duration of purpura by epidermal cooling". Proceedings of SPIE Vol. 2922, "Laser Applications in Medicine and Dentistry", 1996

5 C.J. Chang, B. Anvari, and J.S. Nelson. "Cryogen spray cooling for spatially selective photocoagulation of hemangiomas: a new methodology with preliminary clinical reports". *Plast Reconstr Surg*; 102:459-63, 1998

6 K.M. Kelly, J.S. Nelson, G.P. Lask, R.G. Geronemus, and L.J. Bernstein "Cryogen spray cooling in combination with non-ablative laser treatment of facial rhytides". *Arch Dermatol*; 135:691-4, 1999

7 B. Anvari, T.E. Milner, B.S. Tanenbaum, S. Kimel, L.O. Svaasand, and J.S. Nelson: Selective cooling of biological tissues: application for thermally mediated therapeutic procedures. *Phys Med Biol*, 40:241-52, 1995.

8 J.H. Torres, J.S. Nelson, B.S. Tanenbaum, T.E. Milner, D.M. Goodman, and B Anvari: "Estimation of internal skin temperature measurements in response to cryogen spray cooling: implications for laser therapy of port wine stains". *IEEE J. Special Topics Quant. Elect.* 5(4) pp 1058-1066, 1999

9 C. Sturesson, and S. Andersson-Engels: Mathematical modeling of dynamic cooling and pre-heating, used to increase the depth of selective damage to blood vessels in laser treatment of port wine stains. *Phys Med Biol*, 41:413-28, 1996.

10 W. Verkruysse, B. Majaron, B.S. Tanenbaum, and J.S. Nelson. "Optimal cryogen spray cooling parameters for pulsed laser treatment of port wine stains". *Submitted to Lasers in Surgery and Medicine*.

11 J.W. Valvano and J. Pearce: "Temperature measurements" in Welch AJ and van Gemert MJC. Eds. Optical thermal response of laser irradiated tissue. Plenum Press, New York and London: p515, 1995

12 F.P. Incropera and D.P. DeWitt. Fundamentals of Heat and Mass Transfer. John Wiley & Sons, Inc. New York. 4th edition, p8, 1996.

13 H.H. Zenzie, G.B. Altshuler, M.Z. Smirnov, R.R Anderson, and C.C. Dierickx: Contact or spray cooling: what is the best choice? Oral presentation 3590A-75 at SPIE conference San Jose, CA, 1999.

14 G. Aguilar, W. Verkruysse, B. Majaron, Y. Zhou, J.S. Nelson, and E.J. Lavernia, "Modeling cryogenic Spray Temperature and Evaporation Rate Based on Single-Droplet Analysis", to appear in Proceedings of the Eighth International Conference on Liquid Atomization and Spray Systems, Pasadena, CA, USA, July 2000.

15 H.S. Carslaw and J.C. Jaeger. Conduction of Heat in Solids. Oxford Science Publications. 2nd edition., p 20, 1959.